

# Exploring Neutrino-Nucleus Interactions in the GeV Regime using MINERvA

X.-G. Lu<sup>1,a</sup>, Z. Ahmad Dar<sup>2,3</sup>, F. Akbar<sup>3</sup>, D.A. Andrade<sup>4</sup>, M. V. Ascencio<sup>5</sup>, G.D. Barr<sup>1</sup>, A. Bashyal<sup>6</sup>, L. Bellantoni<sup>7</sup>, A. Bercellie<sup>8</sup>, M. Betancourt<sup>7</sup>, A. Bodek<sup>8</sup>, J. L. Bonilla<sup>4</sup>, H. Budd<sup>8</sup>, G. Caceres<sup>9</sup>, T. Cai<sup>8</sup>, M.F. Carneiro<sup>6,9,b</sup>, H. da Motta<sup>9</sup>, G.A. Díaz<sup>8</sup>, J. Felix<sup>4</sup>, L. Fields<sup>7</sup>, A. Filkins<sup>2</sup>, R. Fine<sup>8,c</sup>, A.M. Gago<sup>5</sup>, H. Gallagher<sup>10</sup>, S.M. Gilligan<sup>6</sup>, R. Gran<sup>11</sup>, D.A. Harris<sup>12,7</sup>, S. Henry<sup>8</sup>, D. Jena<sup>7</sup>, S. Jena<sup>13</sup>, J. Kleykamp<sup>8</sup>, A. Klustová<sup>14</sup>, M. Kordosky<sup>2</sup>, D. Last<sup>15</sup>, A. Lozano<sup>9</sup>, E. Maher<sup>16,d</sup>, S. Manly<sup>8</sup>, W.A. Mann<sup>10</sup>, C. Mauger<sup>15</sup>, K.S. McFarland<sup>8</sup>, A.M. McGowan<sup>8</sup>, B. Messerly<sup>17,e</sup>, J. Miller<sup>18</sup>, J.G. Morfin<sup>7</sup>, D. Naples<sup>17</sup>, J.K. Nelson<sup>2</sup>, C. Nguyen<sup>19</sup>, A. Olivier<sup>8</sup>, V. Paolone<sup>17</sup>, G.N. Perdue<sup>7,8</sup>, K.-J. Plows<sup>1</sup>, M.A. Ramírez<sup>15,4</sup>, R.D. Ransome<sup>20</sup>, H. Ray<sup>19</sup>, P.A. Rodrigues<sup>8,21,1</sup>, D. Ruterbories<sup>8</sup>, H. Schellman<sup>6</sup>, C.J. Solano Salinas<sup>22</sup>, H. Su<sup>17</sup>, M. Sultana<sup>8</sup>, V.S. Syrotenko<sup>10</sup>, E. Valencia<sup>2,4</sup>, A.V. Waldron<sup>14</sup>, D. Wark<sup>1</sup>, A. Weber<sup>1</sup>, K. Yang<sup>1</sup>, and L. Zazueta<sup>2</sup>  
(The MINERvA Collaboration)

<sup>1</sup> University of Oxford, Department of Physics, Oxford, OX1 3PJ United Kingdom

<sup>2</sup> Department of Physics, William & Mary, Williamsburg, Virginia 23187, USA

<sup>3</sup> AMU Campus, Aligarh, Uttar Pradesh 202001, India

<sup>4</sup> Campus León y Campus Guanajuato, Universidad de Guanajuato, Lascurain de Retana No. 5, Colonia Centro, Guanajuato 36000, Guanajuato México.

<sup>5</sup> Sección Física, Departamento de Ciencias, Pontificia Universidad Católica del Perú, Apartado 1761, Lima, Perú

<sup>6</sup> Department of Physics, Oregon State University, Corvallis, Oregon 97331, USA

<sup>7</sup> Fermi National Accelerator Laboratory, Batavia, Illinois 60510, USA

<sup>8</sup> University of Rochester, Rochester, New York 14627 USA

<sup>9</sup> Centro Brasileiro de Pesquisas Físicas, Rua Dr. Xavier Sigaud 150, Urca, Rio de Janeiro, Rio de Janeiro, 22290-180, Brazil

<sup>10</sup> Physics Department, Tufts University, Medford, Massachusetts 02155, USA

<sup>11</sup> Department of Physics, University of Minnesota – Duluth, Duluth, Minnesota 55812, USA

<sup>12</sup> York University, Department of Physics and Astronomy, Toronto, Ontario, M3J 1P3 Canada

<sup>13</sup> Department of Physical Sciences, IISER Mohali, Knowledge City, SAS Nagar, Mohali - 140306, Punjab, India

<sup>14</sup> The Blackett Laboratory, Imperial College London, London SW7 2BW, United Kingdom

<sup>15</sup> Department of Physics and Astronomy, University of Pennsylvania, Philadelphia, PA 19104

<sup>16</sup> Massachusetts College of Liberal Arts, 375 Church Street, North Adams, MA 01247

<sup>17</sup> Department of Physics and Astronomy, University of Pittsburgh, Pittsburgh, Pennsylvania 15260, USA

<sup>18</sup> Departamento de Física, Universidad Técnica Federico Santa María, Avenida España 1680 Casilla 110-V, Valparaíso, Chile

<sup>19</sup> University of Florida, Department of Physics, Gainesville, FL 32611

<sup>20</sup> Rutgers, The State University of New Jersey, Piscataway, New Jersey 08854, USA

<sup>21</sup> University of Mississippi, Oxford, Mississippi 38677, USA

<sup>22</sup> Facultad de Ciencias, Universidad Nacional de Ingeniería, Apartado 31139, Lima, Perú

**Abstract.** With the advance of particle accelerator and detector technologies, the neutrino physics landscape is rapidly expanding. As neutrino oscillation experiments enter the intensity and precision frontiers, neutrino-nucleus interaction measurements are providing crucial input. MINERvA is an experiment at Fermilab dedicated to the study of neutrino-nucleus interactions in the regime of incident neutrino energies from one to few GeV. The experiment recorded neutrino and antineutrino scattering data with the NuMI beamline from 2009 to 2019 using the Low-Energy and Medium-Energy beams that peak at 3 GeV and 6 GeV, respectively. This article reviews the broad spectrum of interesting nuclear and particle physics that MINERvA investigations have illuminated. The newfound, detailed knowledge of neutrino interactions with nuclear targets thereby obtained is proving essential to continued progress in the neutrino physics sector.

## Contents

1	Introduction . . . . .	2
2	MINERvA Experiment and Flux Predictions . . . . .	3
3	Incoherent Neutrino-Nucleus Interactions . . . . .	4
3.1	First Measurements of Quasielastic and Quasielastic-Like Cross Sections . . . . .	5
3.2	Initial-State Correlations and 2p2h-Like Enhancement . . . . .	7
3.3	State-of-the-Art Quasielastic-Like Measurements . . . . .	10
3.4	Charged-Current Pion Production . . . . .	12
3.5	Kaon Production . . . . .	14
3.6	Inelastic Reactions . . . . .	15
4	Coherent Interactions . . . . .	17
5	Conclusions and Outlook . . . . .	18

## 1 Introduction

Neutrinos with energies of a few GeV are involved in many different ways among phenomena that present opportunities to probe fundamental aspects of physical reality. Neutrinos produced in accelerators play a central role in precision measurements of the oscillation parameters such as the Dirac CP-violating phase that may be present in the neutrino flavor mixing matrix [1, 2, 3, 4]. Measurement of a non-zero Dirac phase could unlock the mystery of the matter-antimatter asymmetry of the Universe. Neutrino beams serve as potential sources of beyond-Standard-Model (BSM) particles, such as light dark matter and heavy neutral leptons [5, 6]. On the other hand, neutrinos could impede the discovery of such new forms of matter by mimicking their BSM signatures. This possibility exists because some neutrino SM processes in detector materials have aspects that are poorly known. Atmospheric neutrinos that

<sup>a</sup> e-mail: [xianguo.lu@physics.ox.ac.uk](mailto:xianguo.lu@physics.ox.ac.uk)

<sup>b</sup> Now at Brookhaven National Laboratory

<sup>c</sup> Now at Los Alamos National Laboratory

<sup>d</sup> Department of Physics

<sup>e</sup> Now at University of Minnesota

are born in cosmic-ray-induced hadronic cascades in the upper atmosphere propagate through the Earth [7], presenting complications as well as opportunities for new physics searches. Atmospheric neutrinos oscillate, and their oscillations undergo highly interesting alterations due to propagation through a matter field. However, these highly penetrating particles also create background to rare-event searches (such as proton decay [8,9]) in deep underground experiments. Understanding how a neutrino interacts with a nucleus is essential for exploiting these opportunities. Given that current GeV-neutrino sources (accelerators or atmospheric) are not monoenergetic, these energy-sensitive interactions are convolved with the neutrino flux, causing major systematic uncertainties in precision measurements.

Neutrino-nucleus ( $\nu$ -A) interactions arise not only from the primary nucleon-level interaction, but also from the effect that the nuclear environment exerts on the initial-state nucleons and the final-state particles. Since a theory of the complete nuclear response in neutrino-nucleus interactions in the few-GeV regime of incident neutrino energy is yet to be developed [10], comprehensive  $\nu$ -A measurements are needed to guide and benchmark the development of models. MINERvA (Main INjector Experiment for  $\nu$ -A) at Fermilab is a dedicated experiment to illuminate the interplay between hadronic and nuclear degrees of freedom in  $\nu$ -A interactions and to measure aspects of intranuclear dynamics that are prerequisites for precision neutrino oscillation measurements.

MINERvA received the NuMI (Neutrinos-from-the-Main-Injector) beam at a distance of 1 km from the target of the 120-GeV primary proton beam at Fermilab. In the Low-Energy (LE) beam configurations operated between 2009 and 2012, both the  $\nu_\mu$  and  $\bar{\nu}_\mu$  fluxes peak at  $\sim 3$  GeV, while in the Medium-Energy (ME) configurations used between 2013 and 2019, the fluxes peak at  $\sim 6$  GeV. In both beams, there is a high-energy component that extends beyond 50 GeV. The data collected by MINERvA correspond to 4.0 (1.7) and 12.1 (12.4) times  $10^{20}$  protons on target (POT) for the LE and ME  $\nu_\mu$  ( $\bar{\nu}_\mu$ ) configurations, respectively. In the Sections below, the neutrino interaction physics investigated by MINERvA is reviewed, with the main focus being the techniques developed and measurements reported that are based on the Low-Energy data set.

## 2 MINERvA Experiment and Flux Predictions

The MINERvA detector [11] utilizes extruded plastic scintillator as its tracking medium. Most of the active mass is located in its central polystyrene target whose 5.4-t fiducial volume serves as a charged-particle tracker. The upstream section of the detector consists of a series of passive targets (helium, carbon, water, iron, and lead) interleaved with tracking planes. Sampling calorimeters surround both passive and active target regions. Muons produced by  $\nu$ -A charged-current (CC) interactions in the tracker or in the upstream targets exit the downstream end of the tracker. These muons may then enter and propagate through the magnetized MINOS near detector [12] located 2 m downstream, allowing their trajectories to be momentum-analyzed.

The downstream tracking of muons in the MINOS near detector provides an 8% muon momentum resolution (at 5 GeV/ $c$ ). This complements the three-dimensional tracking and energy-loss measurement of final-state particles that is afforded by the MINERvA tracker. In the tracker, the momentum resolution for protons is 2% at 1 GeV/ $c$  with a 450-MeV/ $c$  tracking threshold. The hadronic energy response of the detector was calibrated using test-beam measurements [13], with pion calorimetric energy resolution in the range 20-30%. Furthermore, the tracker is large compared to the interaction length of the neutrons (approximately 10 cm at 20 MeV) produced

in  $\nu$ -A interactions. The 1.5-MeV detection threshold for measuring energy deposit allows interacting neutrons to be registered for a time-of-flight measurement [14]. The neutron timing resolution is 4.5 ns where the hit resolution alone is 3 ns from electronics effects.

The NuMI beam fluxes used by MINERvA are modeled with GEANT4 predictions that are adjusted to match hadron production data [15]. The large fiducial volume of the MINERvA tracker and the intense beam fluxes make it possible to use neutrino scattering on atomic electrons,  $\bar{\nu}_\mu e^- \rightarrow \bar{\nu}_\mu e^-$ , to further constrain the flux predictions. In the data from the LE (ME) NuMI beam configurations, 135 (810) neutrino-electron scattering events were identified [16, 17]. The constraints thereby provided reduce the  $\nu_\mu$  flux normalization in the *a priori* prediction by 6 % for LE, and 10 % for ME (Fig. 1). Moreover, the uncertainty at the flux peak is reduced from 9 to 6 % for LE, and from 8 to 4 % for ME. In addition, the “low- $\nu$ ” method has been used to constrain the flux shape [18, 19]. The latter method exploits the minimal neutrino energy dependence of the inclusive charged-current cross section at low hadronic recoil energy.

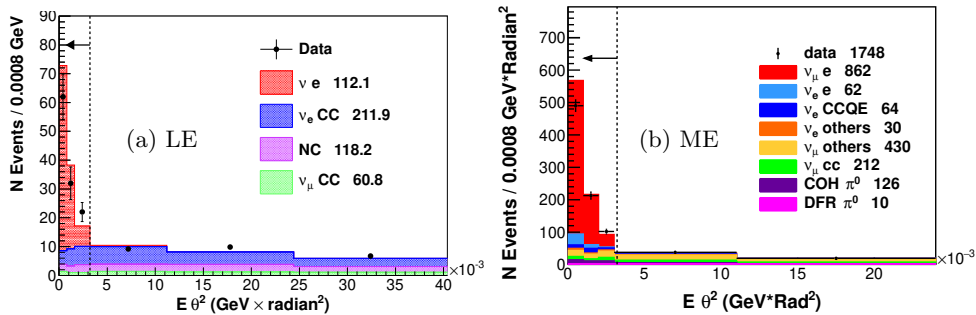


**Fig. 1.** Reconstructed electron energy ( $E$ ) times the square of the electron angle with respect to the beam ( $\theta$ ) for the neutrino-electron elastic scattering candidates with the NuMI (a) LE and (b) ME configurations. Left of the dash lines are the selected samples. Stacked histograms are the simulated event contributions using the *a priori* flux models (NC refers to other neutral-current events that are background). COH and DFR stand for coherent and diffractive production, respectively). Figures from Refs. [16, 17].

### 3 Incoherent Neutrino-Nucleus Interactions

In the few-GeV regime, neutrino-nucleus cross sections are dominated by incoherent processes in which the constituent nucleons can be ejected, possibly accompanied by pions and other mesons. These primary processes are quasielastic (QE), baryon resonance production (RES) including non-resonant background, and deep inelastic scattering (DIS), in ascending order of excitation by incident neutrinos of increasing lab-frame energies. The initial energy and momentum of the struck nucleon and its correlation with other nucleons (including long-range correlations and two-particle-two-hole excitations, or 2p2h [20, 21, 22, 23, 24]) contribute to the initial-state conditions. The primary hadronic final-state particles propagate inside the remnant nucleus and may participate in final-state intranuclear interactions (FSI). The latter interactions may further excite the remaining system, causing nucleon emission or even spallation. Because pions can be absorbed or created during FSI, there is no unique

experimental signature for a given primary process. As a result, the particle content and energy budget of a  $\nu$ -A interaction varies with the initial and final states together with the primary reaction.

By restricting the final-state topology, MINERvA can examine exclusive and semi-inclusive reactions such as mesonless (i.e., quasielastic-like), pion, and kaon production; the experiment can study inclusive scattering as well. The exclusive-channel studies must take into account pion absorption through FSI, which enables resonance production and DIS reactions to be present in quasielastic-like topologies.

The MINERvA data enable the elucidation of one-particle-one-hole mechanisms that are generally used in  $\nu$ -A scattering models, and they also allow examination of the significant 2p2h contributions to the quasielastic-like process. Concerning the latter, MINERvA has identified a 2p2h-like enhancement that simultaneously describes both neutrino and antineutrino scattering data at the kinematic region between quasielastic and resonance production. These unmodeled additional event rates are likely an admixture of all three reactions and their precise nature is still under study.

Decoupling the primary process and medium effects is challenging, especially in a wide-band neutrino beam where the neutrino energy ( $E_\nu$ ) is unknown. In first order, reaction  $E_\nu$ -dependence comes from the primary interactions and the final-state momenta and angles depend strongly on  $E_\nu$ . The nuclear response, on the other hand, affects these elementary distributions as a perturbation; it depends on  $E_\nu$  through the medium coupling to the primary initial-and final-state hadrons. With a neutrino beam where the neutrino direction is precisely known, the kinematics projected onto the transverse plane to the neutrino will have less dependence on  $E_\nu$ .

In a charged-current measurement, certain final-state correlations of the lepton and the hadronic system, such as the transverse kinematic imbalance (TKI) [25,26], avoid or cancel the primary-level dependence on, for example,  $E_\nu$  and axial form factors, and are directly sensitive to the nuclear response with minimal dependence on the neutrino energy. Because exclusivity can be achieved in the transverse plane to the neutrino direction, TKI can probe the hidden dynamics inside the target nucleus. MINERvA has systematically explored the potential of TKI to identify the medium properties and interaction dynamics in exclusive processes.

A review of MINERvA's measurements of incoherent interactions is presented in this section. These measurements encompass both exclusive and elastic reactions to inclusive and inelastic processes.

### 3.1 First Measurements of Quasielastic and Quasielastic-Like Cross Sections

The charged-current quasielastic interaction (CCQE) is an important channel in neutrino oscillation experiments. This interaction gives rise to the majority of events in T2K [1] and to a sizable fraction of the events recorded by NOvA [2]. In quasielastic scattering, the neutrino energy can in principle be inferred from the outgoing lepton kinematics. However, this relatively simple interaction incurs significant effects from the nuclear environment.

Candidate CCQE interactions of neutrinos and antineutrinos on nucleons,  $\nu_\mu n \rightarrow \mu^- p$  and  $\bar{\nu}_\mu p \rightarrow \mu^+ n$ , respectively, were extracted from the Low-Energy data in the first two cross-section measurements reported by MINERvA [27,28]. After subtracting the non-QE background processes, namely resonance production and DIS, the flux-integrated differential cross sections in four-momentum transfer squared,  $Q^2$ , were compared to model predictions by GENIE [29] and NUWRO [30] (Fig. 2). In the neutrino generator predictions, the shape of the  $Q^2$  distribution is parameterized by the axial vector mass,  $M_A$ , plus model representations of the nuclear state (relativistic

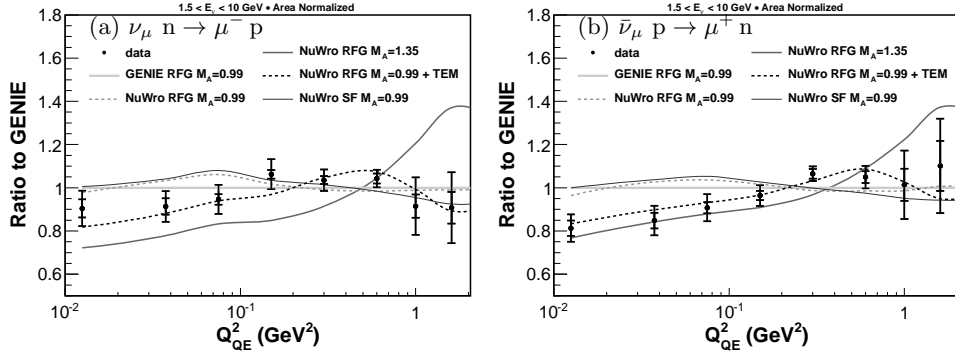


**Fig. 2.** (a) The  $\nu_\mu$  and (b)  $\bar{\nu}_\mu$  CCQE cross section in  $Q_{QE}^2$ . The subscript QE refers to the quasielastic hypothesis that uses only the muon kinematics in the calculation where the target nucleon is assumed to be at rest. The data and model predictions are area-normalized (shape comparison only) and shown as ratios relative to GENIE. Figures from Refs. [27, 28].

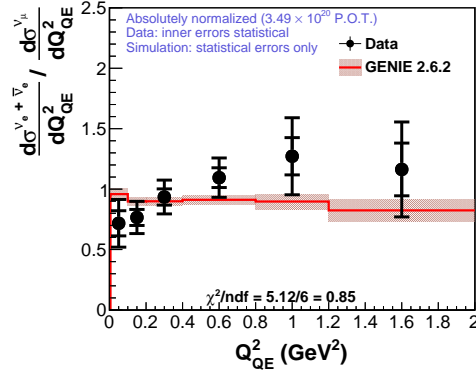


**Fig. 3.** Flux-integrated  $\nu_e$  (dominant) and  $\bar{\nu}_e$  combined CCQE cross section divided by the  $\nu_\mu$  counterpart, compared to the GENIE prediction. Figure from Ref. [34].

Fermi gas, or RFG [31], and Spectral Function, or SF [32]). Both the neutrino and antineutrino data sets were found to favor a parametric enhancement in the magnetic form factor (Transverse Enhancement Model, or TEM [33]), in addition to the *at-that-time-standard* choice of RFG and the world-average  $M_A$  value of  $0.99 \text{ GeV}/c^2$ . Because TEM is extracted from a fit to electron scattering data to describe the contributions from two-nucleon knock-out processes, these results suggest possible contributions from 2p2h in neutrino and antineutrino scattering. This interpretation is further supported by the observed pattern of energy deposits near the interaction vertices (vertex energy) in both measurements.

MINERvA also measured the  $\nu_e$  CCQE cross section in the Low-Energy neutrino data set [34]. In the Standard Model, lepton couplings are universal. However, because the final-state lepton mass is different in  $\nu_e$  versus  $\nu_\mu$  CC events, the nuclei respond to slightly different phase spaces—a difference that cannot be ignored in oscillation experiments [35]. As the CC-induced electrons are reconstructed in the tracker which is charge-insensitive, a flux-averaged cross section including limited contributions from  $\bar{\nu}_e$  is obtained. By comparing to the  $\nu_\mu$  counterpart [28], it has been shown that the

two CCQE cross sections are consistent (Fig. 3). Moreover, GENIE describes the  $\nu_e$ -to- $\nu_\mu$  cross-section ratio within the experimental error which is of order 10-20%.

In MINERvA quasielastic measurements, the inelastic background arising from primary pion production that is followed by absorption during FSI must be subtracted. In subsequent MINERvA studies of the quasielastic dynamics, the inelastic pionless events are instead considered as part of the “QE-like” signal definition in order to mitigate the model uncertainties for pion absorption. In MINERvA’s first QE-like cross-section measurement [36], the  $Q^2$  distribution is extracted. In addition to the change of signal definition, the  $Q^2$  calculation is completely hadron-based, using only the momentum of the leading final-state proton above the tracking threshold. This was the first MINERvA measurement to use reconstructed proton tracks. The distribution is compared to model predictions in order to test different hypotheses concerning initial-state correlations and the data are found to disfavor the modeled correlations (Fig. 4).

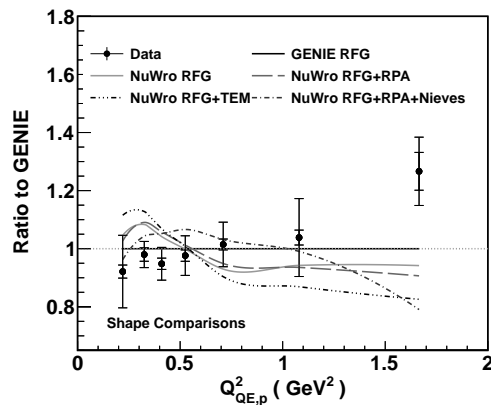


**Fig. 4.** The  $\nu_\mu$  CCQE-like cross section in  $Q^2_{QE,p}$ . The additional subscript p denotes the pure hadronic calculation only using the final-state proton momentum. Comparisons are made to generator predictions that include TEM, Random Phase Approximation (RPA) [37, 38], and the Valencia 2p2h model by Nieves *et al.* [39, 40, 23, 41] (Sect. 3.2). Figure from Ref. [36].

On the other hand, proton kinematics such as the proton-based  $Q^2$  are sensitive to FSI whose strength depends on the size of the target nucleus due to the intranuclear energy loss. This motivated further quasielastic-like cross-section measurements by MINERvA using the detector’s upstream target planes (carbon, iron, and lead) together with the active tracker (CH) [42]. The extracted cross-section ratios of iron and lead to CH are shown in Fig. 5. The data are found to be reasonably well described by the  $A$ -dependent FSI prescriptions used by the GENIE and NuWro event generators.

### 3.2 Initial-State Correlations and 2p2h-Like Enhancement

The nuclear response are often described theoretically using the energy transfer,  $q_0$  (also called  $\omega$  or  $\nu$  in the literature), and the three-momentum transfer,  $q_3$  or  $|\vec{q}|$ , from the lepton to the target nucleus, whereby  $q_3^2 - q_0^2 = Q^2$ . However, the estimation of  $q_0$  experimentally introduces uncertainties due to missing energy from nucleon unbinding and neutrons in the final state. To avoid systematic errors that may enter in this way,

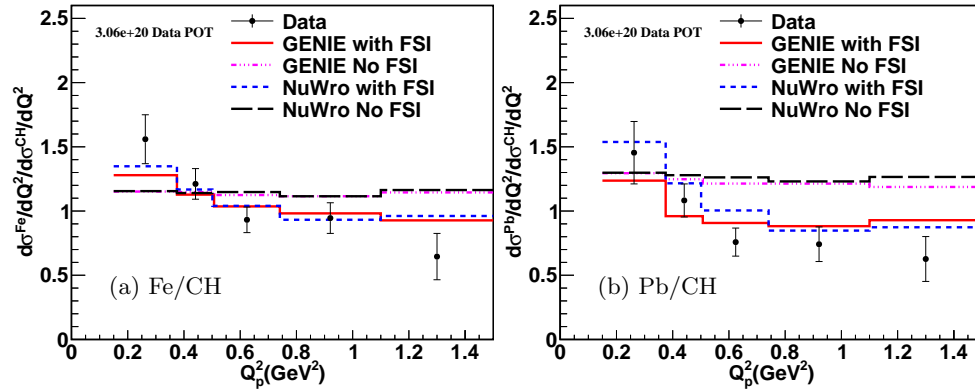


**Fig. 5.** The  $\nu_\mu$  CCQE-like per-nucleon cross sections for (a) iron and (b) lead relative to CH as a function of  $Q^2$ . GENIE and NuWro predictions with RPA and 2p2h models (including the 2p2h-like enhancement discussed in Sect. 3.2) are compared. Figures from Ref. [42].

MINERvA introduced a new observable called “available energy”,  $E_{\text{avail}}$ , as a proxy for  $q_0$  in the “low-recoil” (meaning  $q_3 < 0.8$  GeV) analyses using the Low-Energy  $\nu_\mu$  and  $\bar{\nu}_\mu$  CC inclusive samples [43, 44]. Available energy is defined as the sum of the energies from final-state particles that can be calorimetrically measured in the scintillator and excludes removal energy and neutron energy. An estimate of  $q_0$  is still used with muon kinematics to calculate  $E_\nu$  and then  $q_3$ , but its model uncertainties are subdominant for  $q_3$ .

The measured distributions for reconstructed  $E_{\text{avail}}$  of  $\nu_\mu$  scattering [43] are shown in Fig. 6 (I) for two regions of the reconstructed  $q_3$ . They are compared to the default simulation based on GENIE with modifications to pion production [45, 46]. The simulation is further improved by taking into account initial-state correlations: the collective long-range medium effect in quasielastic events calculated with a Random Phase Approximation (RPA) approach [37], and the Valencia QE-like 2p2h model [39, 40, 23, 41]. Inclusion of RPA brings the event rates at low  $E_{\text{avail}}$  into better agreement with the data, though beyond-Fermi-gas models may have a similar effect [47, 48]. The Valencia 2p2h model helps reduce the model deficit at the dip region between quasielastic and resonance production. The best data-model agreement is achieved by separately scaling up the 2p2h event rates in regions of  $q_0$  and  $q_3$ : across all  $q_0$ - $q_3$  regions, an enhancement by 50% is required to enable the model to match the data, and in the dip region an enhancement of a factor of 2 is needed. Since this *ad hoc* enhancement is based on the Valencia 2p2h model, it was first interpreted as a correction to the modeled 2p2h mechanism. The GENIE model that has evolved to this end is denoted as MNvGENIE in subsequent MINERvA publications.

The corresponding  $\bar{\nu}_\mu$  measurement [44] is shown in Fig. 6 (II), where the aforementioned default simulations and MNvGENIE are compared in (II.a) and (II.b), respectively. Importantly, the 2p2h enhancement in MNvGENIE is only tuned to the  $\nu_\mu$  measurement. Consequently, its predictive power for  $\bar{\nu}_\mu$ , coming from the same underlying  $q_0$ - $q_3$ -dependence as for  $\nu_\mu$ , is intriguing. It suggests that the enhancement is at the level of structure functions rather than of FSI or Fermi motion. However, given its empirical nature, this enhancement should be understood as 2p2h-like; the analysis does not currently rule out a quasielastic or resonant enhancement in addition to 2p2h.

The inclusion of RPA and 2p2h in the predictions has made a significant improvement in the description of the MINERvA data. The evolution of modeling improve-

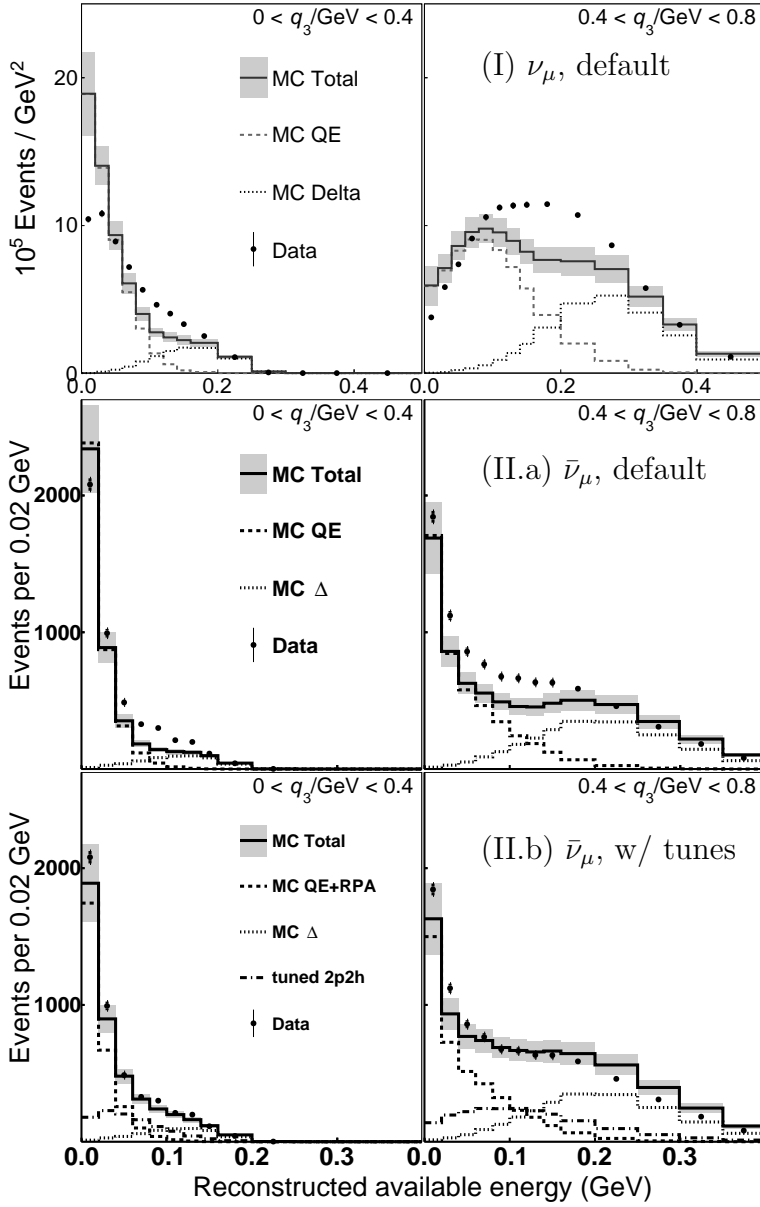


**Fig. 6.** Event distributions in the reconstructed  $E_{\text{avail}}$  for two ranges of the reconstructed  $q_3$  in (I)  $\nu_\mu$  and (II)  $\bar{\nu}_\mu$  charged-current inclusive samples. In (I) and (II.a) the default simulations (see text) are used, while in (II.b) the predictions with the  $\nu_\mu$ -based tunes (MNVGENIE) are shown. In the legend, the resonance region is labeled as Delta ( $\Delta$ ). Figures from Refs. [43,44].

ment from GENIE to MNVGENIE is illustrated by a reanalysis of the vertex energy in a  $\nu_\mu$  CCQE-like sample [49]. As is shown in Fig. 7, the distributions of the reconstructed vertex energies in events with and without proton tracks are described by GENIE after the modifications with RPA, Valencia 2p2h, and the 2p2h-like enhancement are taken into account.

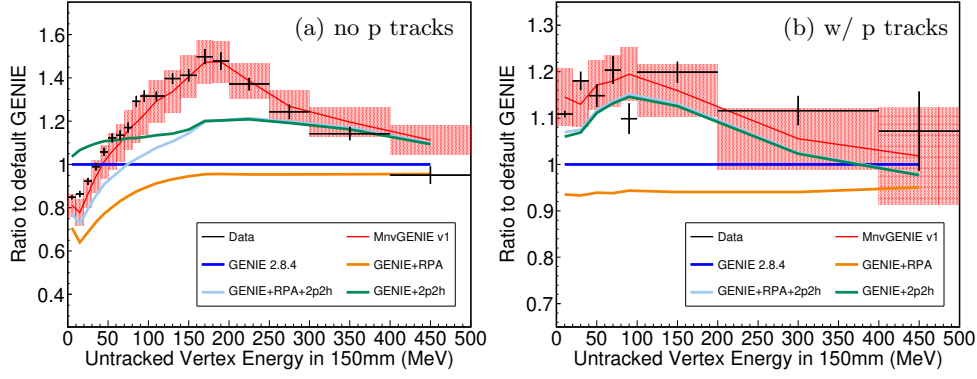


**Fig. 7.** Ratio of the data and various GENIE predictions to GENIE 2.8.4 as a function of the reconstructed vertex energy in  $\nu_\mu$  CCQE-like events (a) without and (b) with proton tracks. The 2p2h-like enhancement can be seen by comparing MnvGENIE and “GENIE+RPA+(Valencia)2p2h”. Figures from Ref. [49].

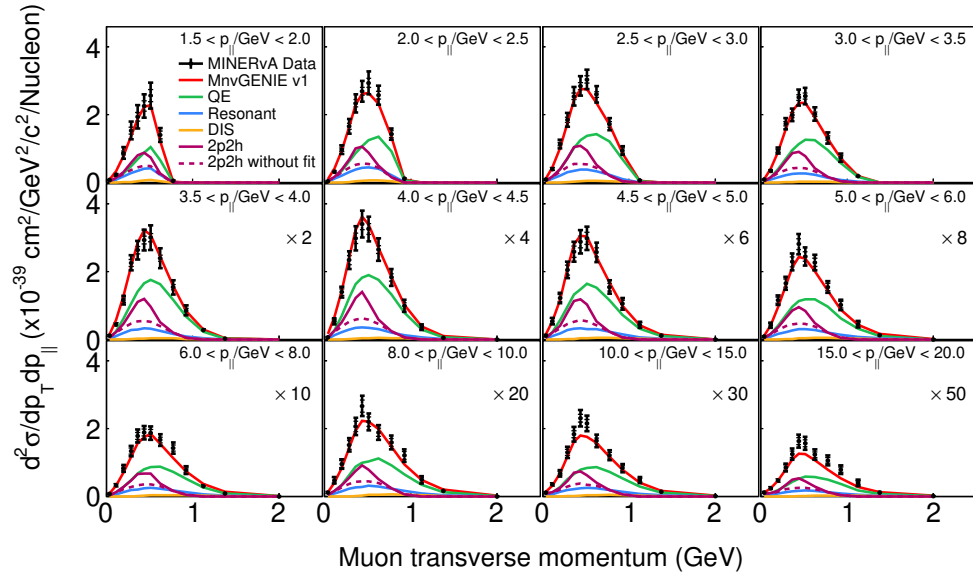


**Fig. 8.**  $\nu_\mu$  CCQE-like cross sections in  $p_T$  in bins of  $p_{||}$ . Unstacked curves show the various components of the MnvGENIE predictions. “2p2h without fit” refers to the Valencia model while “2p2h” includes the *ad hoc* enhancement discussed in Sect. 3.2. Figure from Ref. [49].

### 3.3 State-of-the-Art Quasielastic-Like Measurements

In the few-GeV range of the neutrino energy, the quasielastic cross section is nearly constant as a function of  $E_\nu$ , while the phase space for resonance production and DIS is opening up. In addition to extracting the CCQE-like cross sections in  $Q^2$  and  $E_\nu$  which can be calculated with the quasielastic hypothesis (that is invalid for the non-QE components), MINERvA measured the CC muon transverse ( $p_T$ ) and longitudinal momenta ( $p_{||}$ ) using the Low-Energy  $\bar{\nu}_\mu$  [50],  $\nu_\mu$  [49], and Medium-Energy  $\nu_\mu$  [51] data sets. These particular muon momentum projections respectively approximate the true  $Q^2$  and  $E_\nu$ . As shown in Fig. 8 for the Low-Energy  $\nu_\mu$  results, the different interaction

contributions in the MNvGENIE predictions are relatively stable across the  $p_{||}$  bins. This is in contrast to the inclusive measurement discussed in Sect. 3.6 below where the  $p_{||}$ - (and therefore,  $E_{\nu}$ -) dependence of the DIS processes is evident. In both the QE-like and the inclusive measurements, while MNvGENIE describes the data in most bins, there is an overall model deficit at large  $p_{||}$ .

By measuring the transverse kinematic imbalance which cancel out the primary interaction kinematics, the cross section dependence on the incoming neutrino energy is lessened and also the initial-and final-state effects can be directly probed [26]. Using the  $\nu_{\mu}$  CCQE-like events in the tracker with the Low-Energy data [52], the direction and magnitude of the transverse momentum imbalance ( $\delta\vec{p}_T$ ) between the muon and the leading proton,  $\delta\alpha_T$  and  $\delta p_T$ , respectively, are calculated. The angle  $\delta\alpha_T$  has the most sensitivity to FSI and to the unaccounted-for momentum carried by missing particles such as absorbed pions or the correlated nucleon of the proton from 2p2h. Figure 9 shows that, within the uncertainties, MNvGENIE describes the data. Here, FSI are classified into three categories:

1. A flat distribution for events which do not experience FSI (both the “no-FSI” and “p-FSI non-interacting” categories in Fig. 9) reflecting the isotropy of the Fermi motion;
2. The deceleration region ( $\delta\alpha_T \rightarrow 180^\circ$ ) for energy-dissipating processes—decelerating FSI, pion absorption, and 2p2h;
3. The acceleration region ( $\delta\alpha_T \rightarrow 0^\circ$ ) for accelerating FSI if such a mechanism exists.

Interestingly, GENIE did predict FSI acceleration for protons, roughly half of them singularly occupying the acceleration region, while the other half falls into the deceleration region due to the transverse projection.

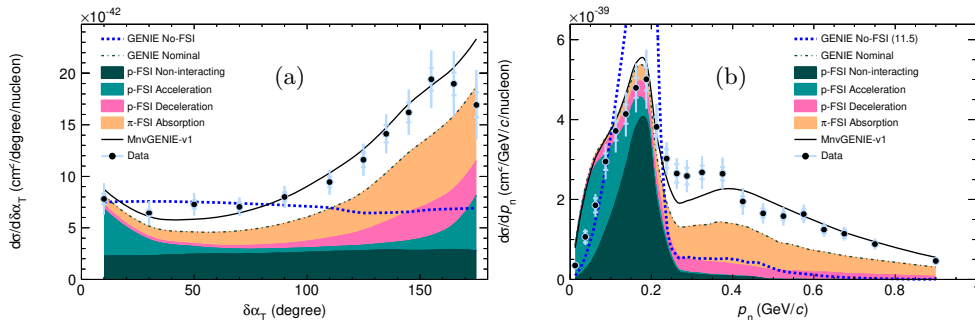


**Fig. 9.** Differential cross sections for  $\nu_{\mu}$  CCQE-like events in (a)  $\delta\alpha_T$  and (b)  $p_n$ . The stacked colored histograms depict categories of FSI and sum up to the GENIE nominal predictions. The predicted 2p2h component including the 2p2h-like enhancement can be inferred from the difference between MNvGENIE and the nominal GENIE. Figures from Ref. [52].

By assuming a carbon-11 target remnant, the transverse momentum imbalance magnitude  $\delta p_T$  is promoted to the three-dimensional momentum imbalance,  $p_n$ , following from an additional constraint by energy conservation [53]. For the FSI-noninteracting events,  $p_n$  can be interpreted as the momentum of the struck neutron in the CCQE initial state. The location of the Fermi-motion peak in data is well captured by the MNvGENIE prediction. However, its accelerating FSI component causes the predicted peak shape to deviate from data. This component was identified as the elastic component of the GENIE v2.8  $hA$  FSI model and has been removed in later versions of GENIE [54, 55]. The measured cross section is further compared to NUWRO

predictions with alternative nuclear states: local Fermi gas (LFG) and Spectral Function. The latter model better describes the Fermi motion peak, but neither model provides enough strength in the transition region between the quasielastic peak and the non-QE tail [52].

An enhanced sensitivity to another initial-state condition, the binding energy, is achieved by further projecting  $\delta\vec{p}_T$  onto the lepton scattering plane, which defines the  $\delta p_{Ty}$  variable [55]. Various generator implementations of the interaction energy on carbon are compared (Fig. 10) and the data favor approximate corrections to GENIE [56].

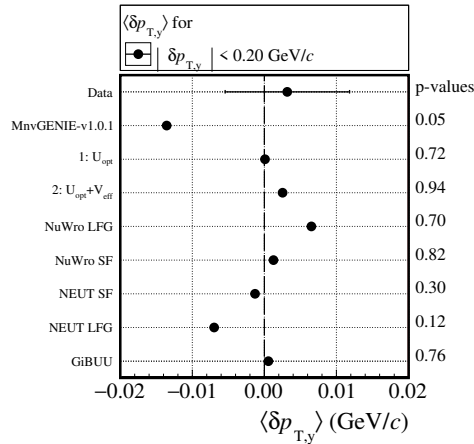


**Fig. 10.** Mean  $\delta p_{Ty}$  calculated from the  $\nu_\mu$  CCQE-like differential cross section in  $\delta p_{Ty}$  within  $-0.20$  to  $0.20$  GeV/c. The  $p$ -value is the probability, assuming normal distribution, that the observed result would have been produced by the test model.  $U_{opt}$  and  $V_{eff}$  are the optical and Coulomb potentials experienced by the CCQE proton and muon, respectively, as proposed in Ref. [56]. NEUT [57] and GiBUU [58] predictions are also compared. Figure from Ref. [55].

### 3.4 Charged-Current Pion Production

Neutrino-induced pion production is an important channel in neutrino oscillation experiments because it accounts for a large part of the signal in NOvA and DUNE [3] far detector event samples, and is both a low-statistics signal and background in the far detector samples of T2K. The process can proceed through baryon resonance production or through non-resonant interaction. It can also occur through a CC coherent interaction with a nucleus—see discussions in Sect. 4. Because of the additional final-state hadrons, incoherent pion production may be more affected by the nuclear environment than the quasielastic process, and the difficulty with reconstructing pions means that the process is harder to measure. One would like to use the lessons learned about nuclear effects in quasielastic-like scattering to (overt) pion production, but the effects may not be the same. The nuclear responses to the pion production fall into three categories according to their relation with those of the quasielastic-like processes:

1. Nuclear responses that are generic but might be quantitatively different in pion production are Fermi motion, binding energy, initial-state correlations, and Pauli blocking [59,60];
2. Pion absorption and charge exchange are nuclear responses that migrate primary pion production channels among each other and into quasielastic-like topology [61,62];
3. Some nuclear responses are specific to pion production such as  $\Delta$ -resonance in-medium modifications [63,64,65].

Moreover, in the energy region of MINERvA, the contribution of higher resonances could be important along with the nuclear medium effects in the pion production processes. MINERvA has measured the following processes on its plastic scintillator tracker with the Low-Energy beam:

- $\nu_\mu$  CC  $\pi^+$  production (with limited contributions from  $\pi^-$ ) [66,67],
- $\nu_\mu$  CC single  $\pi^0$  production [68,69],
- $\bar{\nu}_\mu$  CC single  $\pi^0$  production [70,67], and
- $\bar{\nu}_\mu$  CC single  $\pi^-$  production [71].

The nuclear effects described by RPA and 2p2h are crucial to the description of quasielastic-like processes in MINERvA (Sect. 3.2). Since the RPA effect creates a suppression of the QE-like cross section at low  $Q^2$ , measuring  $Q^2$  in pion production could provide relevant information. However, as shown by the results in Fig. 11, suppression at low  $Q^2$  ranges from being nonexistent ( $\bar{\nu}_\mu \pi^-$  [71]), to mild or insignificant ( $\nu_\mu \pi^+$  [66,67] and  $\bar{\nu}_\mu \pi^0$  [70,67]), and to fairly pronounced ( $\nu_\mu \pi^0$  [68]). A combined fit of the various underlying mechanisms using a subset of these measurements can

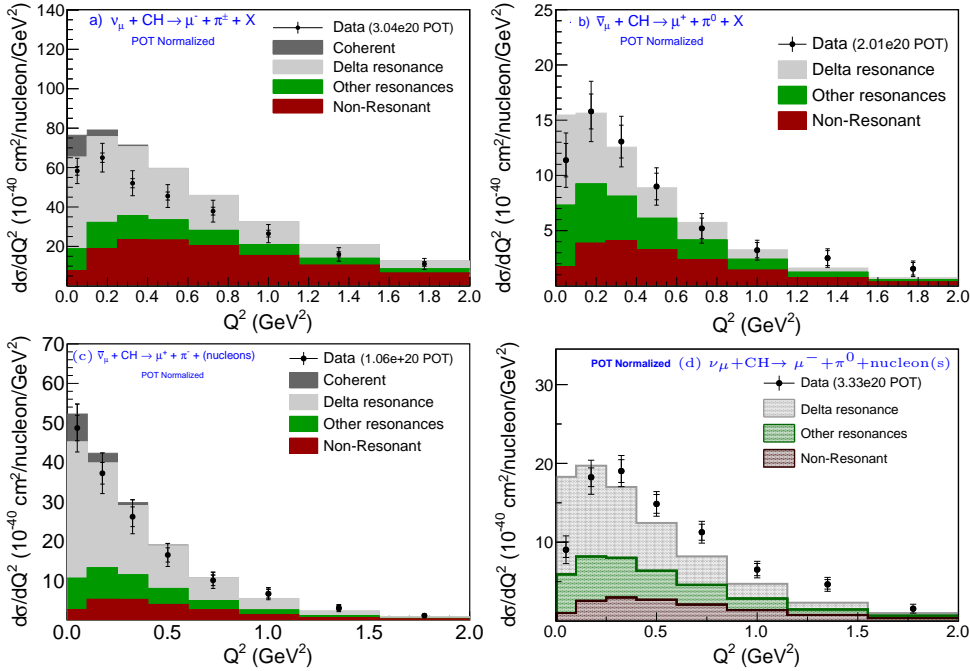


**Fig. 11.** Cross sections in  $Q^2$  for (a)  $\nu_\mu \pi^+$  (with limited contributions from  $\pi^-$ ), (b)  $\bar{\nu}_\mu \pi^0$ , (c)  $\bar{\nu}_\mu \pi^-$ , and (d)  $\nu_\mu \pi^0$  charged-current productions compared to GENIE predictions. Figures from Refs. [67,71,68].

be found in Ref. [72]. On the other hand, while 2p2h in pion production has not been incorporated into predictions, current models describe the MINERvA data with sufficient strength without it. The effect of initial-state correlations on pion production is not well understood.

Because of the granularity of the tracker and the event statistics obtained for  $\nu_\mu$  charged-current proton- $\pi^0$  final states with the Low-Energy beam, MINERvA is able to investigate the transverse kinematic imbalances that may arise in pion production [69]. In this way, MINERvA can probe the initial state and FSI in parallel to the CCQE-like measurement discussed in Sect. 3.3 (Fig. 12). The TKI between the muon and the p- $\pi^0$  hadronic system is calculated by reconstructing the  $\pi^0$  momentum and combining it with the proton momentum [73]. As with  $\nu_\mu$  CCQE, this channel also has an initial-state neutron and as expected, the Fermi motion peaks in Fig. 12 (b) from both channels are consistent. The consistency in the  $p_n$  tail size and in the trend of  $\delta\alpha_T$  in Fig. 12 is purely coincidental. As a specific example, if nature had less pion absorption, the QE-like  $p_n$  tail and the  $\delta\alpha_T$  deceleration region would fall but the overall  $\pi^0$  production would increase. Currently, for the same Fermi motion peak, generator model predictions do not describe both channels simultaneously [69], clearly illustrating the challenges inherent to consistent modeling of few-GeV  $\nu$ -A interactions.

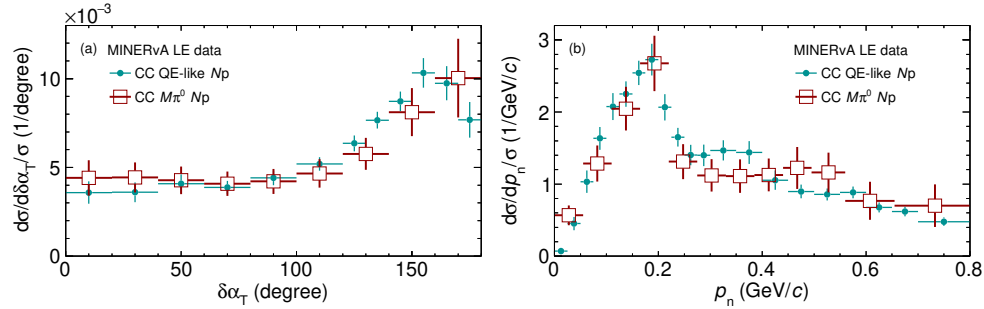


**Fig. 12.** Differential cross sections in (a)  $\delta\alpha_T$  and (b)  $p_n$  for  $\nu_\mu$  charged-current  $p$ - $\pi^0$  production, compared to quasielastic-like scattering [52,55] (Sect. 3.3). The data sets are area-normalized. Figures from Ref. [69].

### 3.5 Kaon Production

Charged and neutral kaons are produced in both charged-current and neutral-current interactions at the beam energies of the MINERvA exposures. Kaon production is important to measure because the neutral-current (NC) channels yielding  $K^+$  mesons constitute a background to proton decay searches [8,9]. This background arises from interactions of atmospheric neutrinos that are incident on proton decay detectors. The production mechanism is associated production with another strange meson or with a hyperon. Below the threshold of associated particle production, kaon production would take place through  $\Delta S = 1$  currents ( $S$  is the strangeness quantum number). At the energies of present interest, single kaon production may be important [74]. A final-state  $K^+$  with energy less than  $\sim 600$  MeV can stop inside the MINERvA tracker and then decay at rest. Once a  $K^+$  decay chain is identified through the decay-associated time delay, the event topology, and the energy loss, the  $K^+$  initial momentum can be

calculated from track range. For neutral-current interactions, the final-state lepton does not identify the vertex location, consequently the 100-MeV tracking threshold sets a lower limit on the measured kaon kinetic energy. For CC interactions on the other hand, the final-state muon determines the primary vertex as the  $K^+$  starting point, hence the kaon kinetic energy threshold can be lower since a kaon track needs not be identified. Figure 13 shows the measured charged-current [75] and neutral-current [76] cross sections. The analysis showed that the GENIE prediction was in agreement with the neutral-current measurement, while the NEUT prediction, which was used by Super-K [8], predicted a lower cross section by about 20 %.

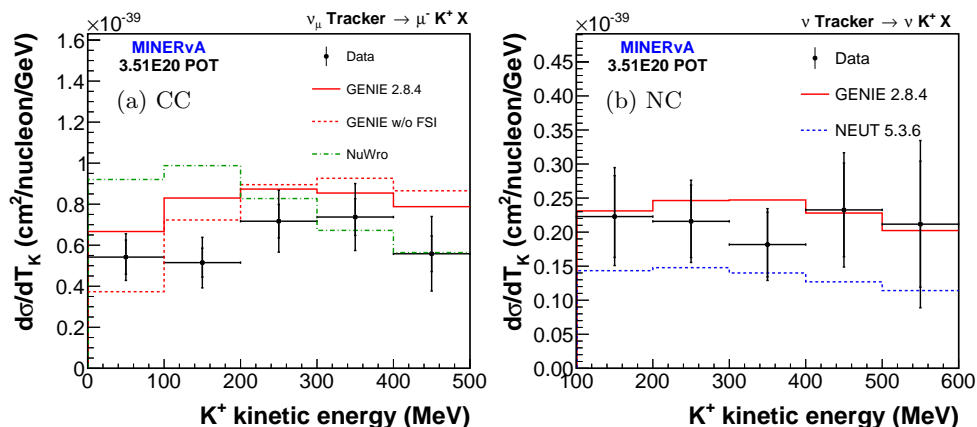


**Fig. 13.** Charged-current (a) and neutral-current (b)  $\nu_\mu$   $K^+$  production cross sections in kinetic energy, compared to GENIE, NUWRO, and NEUT predictions. Figures from Refs. [75, 76].

### 3.6 Inelastic Reactions

In quasielastic and resonance production, the dynamic degrees of freedom are baryons and mesons. The invariant mass of the hadronic system,  $W$ , is of the order of 1-2  $\text{GeV}/c^2$ . In the high- $W$  high- $Q^2$  region where DIS dominates, the target nucleon breaks up in the reaction and the QCD dynamics in the nuclear environment can be studied. This kinematic region is only accessible in inclusive measurements where any hadronic final state is allowed.

MINERvA measures CC inclusive cross sections using the muon kinematics. These measurements require one momentum-analyzed muon per event; no requirement is placed on the final-state hadronic system [77]. Figure 14 shows the  $p_{||}$ -evolution of the inclusive  $p_T$  spectra. In contrast to the CCQE-like measurement of Fig. 8 of Sect. 3.3, there are significant contributions from (GENIE) DIS in all  $p_{||}$  bins and its relative contribution increases with  $p_{||}$ . As in the CCQE-like case, there is an overall deficit of MNVGENIE at large  $p_{||}$ .

Charged-current inclusive cross sections have also been measured in the passive target region as a function of the reconstructed Bjorken- $x$ . These measurements are carried out for iron and lead targets; they are based on both muon kinematics and calorimetric hadronic energy [78]. The ratios of  $\nu_\mu$ -Fe and  $\nu_\mu$ -Pb cross section to the cross section in the tracker (CH) are shown in Fig. 15. The default GENIE simulations

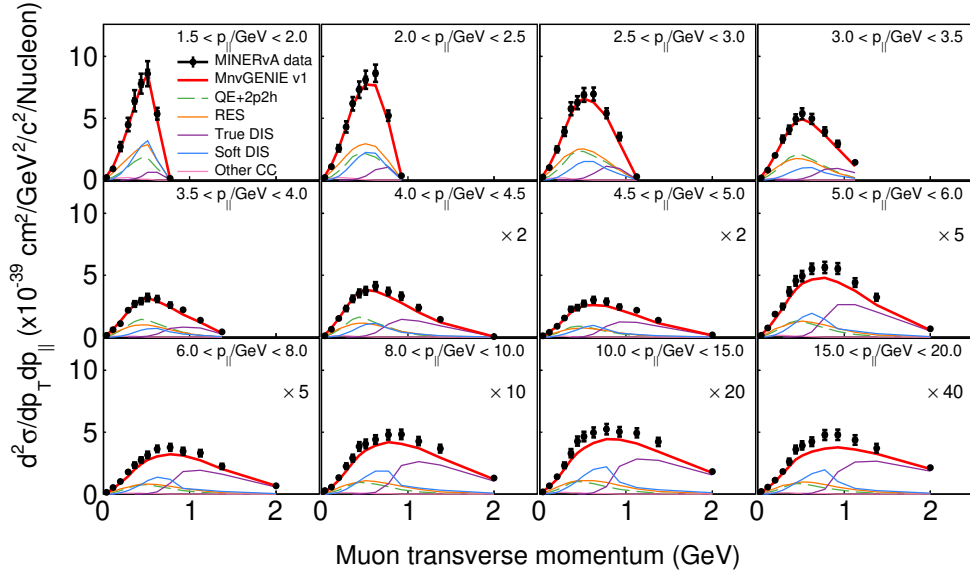


**Fig. 14.**  $\nu_\mu$  charged-current inclusive cross sections in  $p_T$  in bins of  $p_{\parallel}$  compared to MnvGENIE predictions with unstacked contributions shown. See Fig. 8 for comparison. “True DIS” events are defined as GENIE DIS events that satisfy  $W > 2 \text{ GeV}/c^2$  and  $Q^2 > 1 \text{ GeV}^2$ . “Soft DIS” is defined to contain the remaining GENIE DIS events. Figure from Ref. [77].

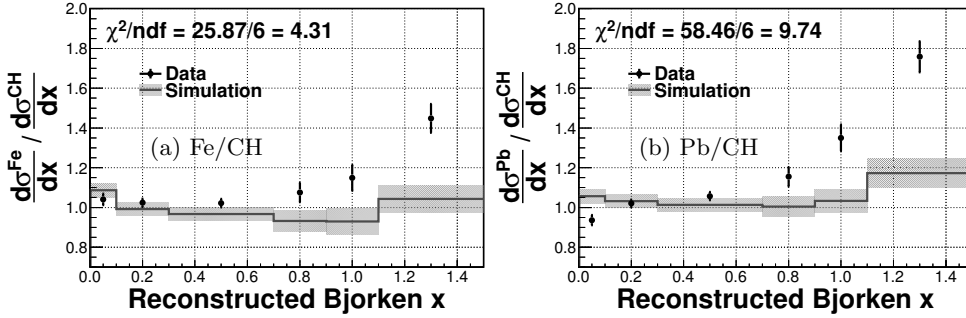


**Fig. 15.** Ratios of  $\nu_\mu$  charged-current inclusive cross sections per nucleon as a function of the reconstructed Bjorken- $x$  for (a) Fe/CH and (b) Pb/CH, compared to the default GENIE simulations. Figures from Ref. [78].

show a strong deficit in the elastic region (Bjorken- $x \sim 1$ ) which might be due to the unmodeled 2p2h contributions.

By restricting the sample to the DIS region,  $W > 2 \text{ GeV}/c^2$  and  $Q^2 > 1 \text{ GeV}^2$ , these Bjorken- $x$ -dependent cross section ratios can be compared to additional DIS models [79] (Fig. 16). As is shown in Fig. 16 (b) for Pb, the data at Bjorken- $x < 0.1$  suggests possible shadowing effects beyond those predicted. Because these models are only tuned to charged-lepton scattering data, which are by definition insensitive to the axial-vector current, these data also reflect neutrino-specific effects in the DIS region.

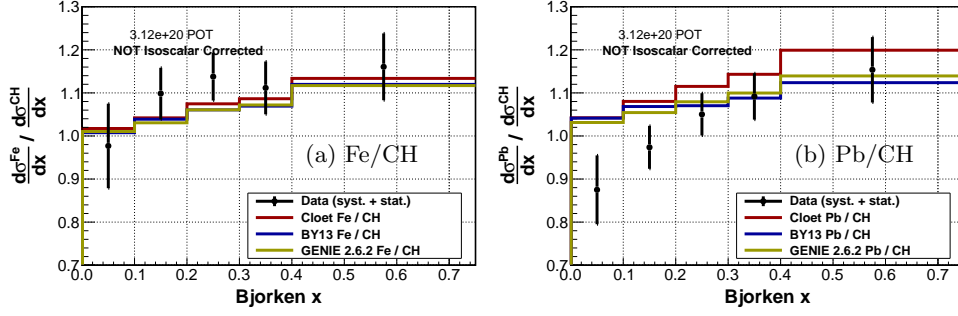


**Fig. 16.** Ratios of  $\nu_\mu$  charged-current DIS cross sections per nucleon as a function of Bjorken- $x$  for (a) Fe/CH and (b) Pb/CH, compared to the default GENIE, Bodek-Yang (BY13) [80], and Cloet [81] models. Figures from Ref. [79].

## 4 Coherent Interactions

Coherent pion production is a relatively rare process that is worthy of measurement because the neutral-current channel contributes a small but poorly constrained background to electron neutrino appearance measurements. Charged-current coherent pion production,  $\bar{\nu}_\mu + A \rightarrow \mu^+ + \pi^- + A$ , can be considered as the inverse process of the pion decay permitted in a nuclear environment, in analogy to pair production in QED. The momentum transfer from the pion to the nucleus—denoted by  $t \equiv (P' - P)^2$  where  $P'$  and  $P$  are the final and initial 4-momenta of the nucleus—is small and leaves the nucleus intact, and the process has a characteristic exponential fall-off of the cross section with increasing  $|t|$ . By reconstructing  $t$ , MINERvA measured this process with both  $\nu_\mu$  and  $\bar{\nu}_\mu$  beams [82]. This measurement has provided a critical validation of the model implementation in generators (Fig. 17). Further model comparisons in a reanalysis [83] show preference for the Berger-Sehgal model [84] over the Rein-Sehgal model [85,86] used by GENIE. In the low energy region, explicit

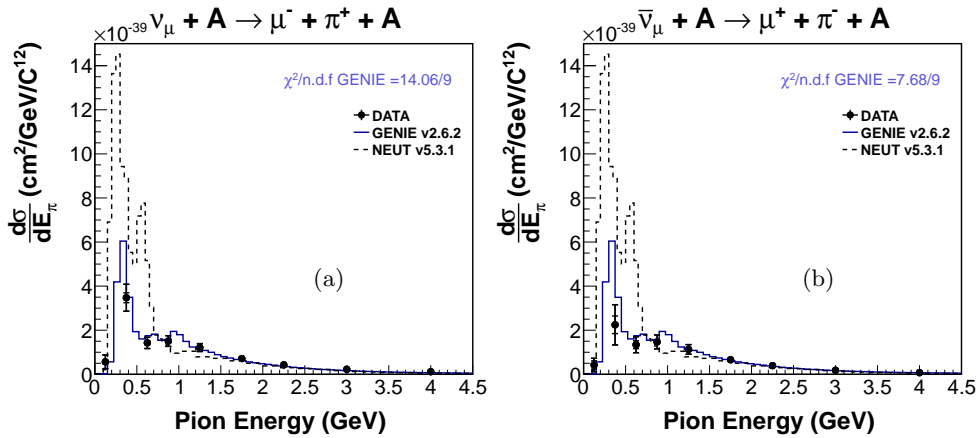


**Fig. 17.** Charged-current coherent pion production cross sections as a function of the pion energy in (a)  $\nu_\mu$  and (b)  $\bar{\nu}_\mu$  scattering, compared to the Rein-Sehgal model predictions implemented in GENIE and NEUT. Figures from Ref. [82].

nuclear model has been used to study coherent pion production (see, for example, Refs. [87, 88]).

The  $t$ -measurement was augmented with  $K^+$  tagging (Sect. 3.5) in order to search for the analogous kaon production,  $\nu_\mu + A \rightarrow \mu^- + K^+ + A$ . MINERvA found 6 candidates with 1.77 predicted background events. This observation comprises evidence at  $3.0\sigma$  that CC coherent  $K^+$  production does indeed occur [89].

A process that is the analog of neutrino NC coherent  $\pi^0$  production on nuclei, is neutrino diffractive  $\pi^0$  production on hydrogen:  $\bar{\nu} + H \rightarrow \bar{\nu} + \pi^0 + H$ . This reaction relies solely on vacuum-quantum-number (Pomeron) exchange, hence diffractive [90]. In the past, diffractive  $\pi^0$  production on hydrogen was not included in neutrino event generators. It has been identified by MINERvA as the cause of a data excess observed in neutral-current events containing electromagnetic showers in the tracker [91].

## 5 Conclusions and Outlook

With the NuMI Low-Energy data, MINERvA has investigated a wide variety of neutrino interactions in the GeV region of incident neutrino and antineutrino energies, including elastic scattering on electrons as well as neutrino-nucleus incoherent and coherent scattering processes. The reported measurements include utilization of neutrino scattering observations to constrain the flux, precision measurements of model parameters and model validation, and discoveries of novel processes. The results show neutrino-nucleus interactions to involve complex phenomena which challenge many of the current theoretical descriptions. Incremental improvements to the models have been essential to progress with MINERvA data and interpretation. The experiment's Medium-Energy data, analyses of which are currently underway, will enable comparisons of interaction channels on a range of nuclei at new levels of statistical precision, and expansion to kinematic phase space that has heretofore not been accessible. These data, consolidated by a preservation campaign [92, 93], will not only facilitate future precision measurements of neutrino oscillations, but also further extend the knowledge of electroweak phenomena that lie at the intersection of nuclear and particle physics.

## Acknowledgments

This document was prepared by members of the MINERvA Collaboration using the resources of the Fermi National Accelerator Laboratory (Fermilab), a U.S. Department of Energy, Office of Science, HEP User Facility. Fermilab is managed by Fermi Research Alliance, LLC (FRA), acting under Contract No. DE-AC02-07CH11359. These resources included support for the MINERvA construction project, and support for construction also was granted by the United States National Science Foundation under Award No. PHY-0619727 and by the University of Rochester. Support for participating scientists was provided by NSF and DOE (USA); by CAPES and CNPq (Brazil); by CoNaCyT (Mexico); by Proyecto Basal FB 0821, CONICYT PIA ACT1413, and Fondecyt 3170845 and 11130133 (Chile); by CONCYTEC (Consejo Nacional de Ciencia, Tecnología e Innovación Tecnológica), DGI-PUCP (Dirección de Gestión de la Investigación - Pontificia Universidad Católica del Perú), and VRI-UNI (Vice-Rectorate for Research of National University of Engineering) (Peru); NCN Opus Grant No. 2016/21/B/ST2/01092 (Poland); by Science and Technology Facilities Council (UK); by EU Horizon 2020 Marie Skłodowska-Curie Action; by a Cottrell Postdoctoral Fellowship from the Research Corporation for Scientific Advancement; by an Imperial College London President's PhD Scholarship. We thank the MINOS

Collaboration for use of its near detector data. Finally, we thank the staff of Fermilab for support of the beam line, the detector, and computing infrastructure.

## References

1. K. Abe *et al.*, “Constraint on the matter–antimatter symmetry-violating phase in neutrino oscillations,” *Nature*, vol. 580, no. 7803, pp. 339–344, 2020.
2. M. A. Acero *et al.*, “First Measurement of Neutrino Oscillation Parameters using Neutrinos and Antineutrinos by NOvA,” *Phys. Rev. Lett.*, vol. 123, no. 15, p. 151803, 2019.
3. B. Abi *et al.*, “Deep Underground Neutrino Experiment (DUNE), Far Detector Technical Design Report, Volume I Introduction to DUNE,” *JINST*, vol. 15, no. 08, p. T08008, 2020.
4. K. Abe *et al.*, “Hyper-Kamiokande Design Report,” 2018.
5. K. Abe *et al.*, “Search for heavy neutrinos with the T2K near detector ND280,” *Phys. Rev.*, vol. D100, no. 5, p. 052006, 2019.
6. B. Abi *et al.*, “Prospects for beyond the Standard Model physics searches at the Deep Underground Neutrino Experiment,” *Eur. Phys. J.*, vol. C81, no. 4, p. 322, 2021.
7. K. Abe *et al.*, “Atmospheric neutrino oscillation analysis with external constraints in Super-Kamiokande I-IV,” *Phys. Rev.*, vol. D97, no. 7, p. 072001, 2018.
8. K. Abe *et al.*, “Search for proton decay via  $p \rightarrow \nu K^+$  using 260 kiloton-year data of Super-Kamiokande,” *Phys. Rev.*, vol. D90, no. 7, p. 072005, 2014.
9. F. An *et al.*, “Neutrino Physics with JUNO,” *J. Phys.*, vol. G43, no. 3, p. 030401, 2016.
10. L. Alvarez-Ruso *et al.*, “NuSTEC 1.1 Neutrino Scattering Theory Experiment Collaboration <http://nustec.fnal.gov>. White Paper: Status and challenges of neutrino–nucleus scattering,” *Prog. Part. Nucl. Phys.*, vol. 100, pp. 1–68, 2018.
11. L. Aliaga *et al.*, “Design, Calibration, and Performance of the MINERvA Detector,” *Nucl. Instrum. Meth.*, vol. A743, pp. 130–159, 2014.
12. D. G. Michael *et al.*, “The Magnetized steel and scintillator calorimeters of the MINOS experiment,” *Nucl. Instrum. Meth. A*, vol. 596, pp. 190–228, 2008.
13. L. Aliaga *et al.*, “MINERvA neutrino detector response measured with test beam data,” *Nucl. Instrum. Meth.*, vol. A789, pp. 28–42, 2015.
14. M. Elkins *et al.*, “Neutron measurements from antineutrino hydrocarbon reactions,” *Phys. Rev.*, vol. D100, no. 5, p. 052002, 2019.
15. L. Aliaga *et al.*, “Neutrino Flux Predictions for the NuMI Beam,” *Phys. Rev.*, vol. D94, no. 9, p. 092005, 2016. [Addendum: *Phys. Rev.*D95,no.3,039903(2017)].
16. J. Park *et al.*, “Measurement of Neutrino Flux from Neutrino-Electron Elastic Scattering,” *Phys. Rev.*, vol. D93, no. 11, p. 112007, 2016.
17. E. Valencia *et al.*, “Constraint of the MINERvA medium energy neutrino flux using neutrino-electron elastic scattering,” *Phys. Rev.*, vol. D100, no. 9, p. 092001, 2019.
18. J. Devan *et al.*, “Measurements of the Inclusive Neutrino and Antineutrino Charged Current Cross Sections in MINERvA Using the Low- $\nu$  Flux Method,” *Phys. Rev.*, vol. D94, no. 11, p. 112007, 2016.
19. L. Ren *et al.*, “Measurement of the antineutrino to neutrino charged-current interaction cross section ratio in MINERvA,” *Phys. Rev.*, vol. D95, no. 7, p. 072009, 2017. [Addendum: *Phys. Rev.*D97,no.1,019902(2018)].
20. J. Marteau, “Effects of the nuclear correlations on the neutrino oxygen interactions,” *Eur. Phys. J. A*, vol. 5, pp. 183–190, 1999.
21. M. Martini, M. Ericson, G. Chanfray, and J. Marteau, “Neutrino and antineutrino quasielastic interactions with nuclei,” *Phys. Rev. C*, vol. 81, p. 045502, 2010.
22. J. Nieves, I. Ruiz Simo, and M. J. Vicente Vacas, “Inclusive Charged-Current Neutrino-Nucleus Reactions,” *Phys. Rev. C*, vol. 83, p. 045501, 2011.
23. R. Gran, J. Nieves, F. Sanchez, and M. J. Vicente Vacas, “Neutrino-nucleus quasi-elastic and 2p2h interactions up to 10 GeV,” *Phys. Rev. D*, vol. 88, no. 11, p. 113007, 2013.
24. O. Benhar, A. Lovato, and N. Rocco, “Contribution of two-particle–two-hole final states to the nuclear response,” *Phys. Rev. C*, vol. 92, no. 2, p. 024602, 2015.

25. X.-G. Lu, D. Coplowe, R. Shah, G. Barr, D. Wark, and A. Weber, “Reconstruction of Energy Spectra of Neutrino Beams Independent of Nuclear Effects,” *Phys. Rev.*, vol. D92, no. 5, p. 051302, 2015.
26. X.-G. Lu, L. Pickering, S. Dolan, G. Barr, D. Coplowe, Y. Uchida, D. Wark, M. O. Wascko, A. Weber, and T. Yuan, “Measurement of nuclear effects in neutrino interactions with minimal dependence on neutrino energy,” *Phys. Rev.*, vol. C94, no. 1, p. 015503, 2016.
27. L. Fields *et al.*, “Measurement of Muon Antineutrino Quasielastic Scattering on a Hydrocarbon Target at  $E_\nu \sim 3.5$  GeV,” *Phys. Rev. Lett.*, vol. 111, no. 2, p. 022501, 2013.
28. G. A. Fiorentini *et al.*, “Measurement of Muon Neutrino Quasielastic Scattering on a Hydrocarbon Target at  $E_\nu \sim 3.5$  GeV,” *Phys. Rev. Lett.*, vol. 111, p. 022502, 2013.
29. C. Andreopoulos *et al.*, “The GENIE Neutrino Monte Carlo Generator,” *Nucl. Instrum. Meth.*, vol. A614, pp. 87–104, 2010.
30. T. Golan, C. Juszczak, and J. T. Sobczyk, “Final State Interactions Effects in Neutrino-Nucleus Interactions,” *Phys. Rev.*, vol. C86, p. 015505, 2012.
31. A. Bodek and J. L. Ritchie, “Fermi Motion Effects in Deep Inelastic Lepton Scattering from Nuclear Targets,” *Phys. Rev.*, vol. D23, p. 1070, 1981.
32. O. Benhar, A. Fabrocini, S. Fantoni, and I. Sick, “Spectral function of finite nuclei and scattering of GeV electrons,” *Nucl. Phys.*, vol. A579, pp. 493–517, 1994.
33. A. Bodek, H. S. Budd, and M. E. Christy, “Neutrino Quasielastic Scattering on Nuclear Targets: Parametrizing Transverse Enhancement (Meson Exchange Currents),” *Eur. Phys. J.*, vol. C71, p. 1726, 2011.
34. J. Wolcott *et al.*, “Measurement of electron neutrino quasielastic and quasielasticlike scattering on hydrocarbon at  $\langle E_\nu \rangle = 3.6$  GeV,” *Phys. Rev. Lett.*, vol. 116, no. 8, p. 081802, 2016.
35. M. Day and K. S. McFarland, “Differences in Quasi-Elastic Cross-Sections of Muon and Electron Neutrinos,” *Phys. Rev. D*, vol. 86, p. 053003, 2012.
36. T. Walton *et al.*, “Measurement of muon plus proton final states in  $\nu_\mu$  interactions on hydrocarbon at  $\langle E_\nu \rangle = 4.2$  GeV,” *Phys. Rev.*, vol. D91, no. 7, p. 071301, 2015.
37. J. Nieves, J. E. Amaro, and M. Valverde, “Inclusive quasi-elastic neutrino reactions,” *Phys. Rev.*, vol. C70, p. 055503, 2004. [Erratum: *Phys. Rev. C*72,019902(2005)].
38. K. M. Graczyk and J. T. Sobczyk, “The Algebraic solution of RPA equations for the charged current quasielastic neutrino nucleus scattering,” *Eur. Phys. J. C*, vol. 31, pp. 177–185, 2003.
39. J. Nieves, I. Ruiz Simo, and M. J. Vicente Vacas, “The nucleon axial mass and the MiniBooNE Quasielastic Neutrino-Nucleus Scattering problem,” *Phys. Lett.*, vol. B707, pp. 72–75, 2012.
40. J. T. Sobczyk, “Multinucleon ejection model for Meson Exchange Current neutrino interactions,” *Phys. Rev. C*, vol. 86, p. 015504, 2012.
41. J. Schwehr, D. Cherdack, and R. Gran, “GENIE implementation of IFIC Valencia model for QE-like 2p2h neutrino-nucleus cross section,” 1 2016.
42. M. Betancourt *et al.*, “Direct Measurement of Nuclear Dependence of Charged Current Quasielasticlike Neutrino Interactions Using MINER $\nu$ A,” *Phys. Rev. Lett.*, vol. 119, no. 8, p. 082001, 2017.
43. P. A. Rodrigues *et al.*, “Identification of nuclear effects in neutrino-carbon interactions at low three-momentum transfer,” *Phys. Rev. Lett.*, vol. 116, p. 071802, 2016. [Addendum: *Phys. Rev. Lett.*121,no.20,209902(2018)].
44. R. Gran *et al.*, “Antineutrino Charged-Current Reactions on Hydrocarbon with Low Momentum Transfer,” *Phys. Rev. Lett.*, vol. 120, no. 22, p. 221805, 2018.
45. C. Wilkinson, P. Rodrigues, S. Cartwright, L. Thompson, and K. McFarland, “Reanalysis of bubble chamber measurements of muon-neutrino induced single pion production,” *Phys. Rev. D*, vol. 90, no. 11, p. 112017, 2014.
46. P. Rodrigues, C. Wilkinson, and K. McFarland, “Constraining the GENIE model of neutrino-induced single pion production using reanalyzed bubble chamber data,” *Eur. Phys. J. C*, vol. 76, no. 8, p. 474, 2016.

47. M. Martini, N. Jachowicz, M. Ericson, V. Pandey, T. Van Cuyck, and N. Van Des-  
sel, “Electron-neutrino scattering off nuclei from two different theoretical perspectives,”  
*Phys. Rev. C*, vol. 94, no. 1, p. 015501, 2016.
48. J. Nieves and J. E. Sobczyk, “In medium dispersion relation effects in nuclear inclusive  
reactions at intermediate and low energies,” *Annals Phys.*, vol. 383, pp. 455–496, 2017.
49. D. Ruterbories *et al.*, “Measurement of Quasielastic-Like Neutrino Scattering at  $\langle E_\nu \rangle \sim$   
3.5 GeV on a Hydrocarbon Target,” *Phys. Rev.*, vol. D99, no. 1, p. 012004, 2019.
50. C. E. Patrick *et al.*, “Measurement of the Muon Antineutrino Double-Differential Cross  
Section for Quasielastic-like Scattering on Hydrocarbon at  $E_\nu \sim 3.5\text{GeV}$ ,” *Phys. Rev.*,  
vol. D97, no. 5, p. 052002, 2018.
51. M. F. Carneiro *et al.*, “High-Statistics Measurement of Neutrino Quasielasticlike Scat-  
tering at 6 GeV on a Hydrocarbon Target,” *Phys. Rev. Lett.*, vol. 124, no. 12, p. 121801,  
2020.
52. X.-G. Lu *et al.*, “Measurement of final-state correlations in neutrino muon-proton meson-  
less production on hydrocarbon at  $\langle E_\nu \rangle = 3\text{ GeV}$ ,” *Phys. Rev. Lett.*, vol. 121, no. 2,  
p. 022504, 2018.
53. A. P. Furmanski and J. T. Sobczyk, “Neutrino energy reconstruction from one muon  
and one proton events,” *Phys. Rev. C*, vol. 95, no. 6, p. 065501, 2017.
54. L. Harewood and R. Gran, “Elastic hadron-nucleus scattering in neutrino-nucleus reac-  
tions and transverse kinematics measurements,” 6 2019.
55. T. Cai *et al.*, “Nucleon binding energy and transverse momentum imbalance in neutrino-  
nucleus reactions,” *Phys. Rev.*, vol. D101, no. 9, p. 092001, 2020.
56. A. Bodek and T. Cai, “Removal Energies and Final State Interaction in Lepton Nucleus  
Scattering,” *Eur. Phys. J.*, vol. C79, no. 4, p. 293, 2019.
57. Y. Hayato, “A neutrino interaction simulation program library NEUT,” *Acta Phys.*  
*Polon. B*, vol. 40, pp. 2477–2489, 2009.
58. O. Buss, T. Gaitanos, K. Gallmeister, H. van Hees, M. Kaskulov, O. Lalakulich, A. B.  
Larionov, T. Leitner, J. Weil, and U. Mosel, “Transport-theoretical Description of Nu-  
clear Reactions,” *Phys. Rept.*, vol. 512, pp. 1–124, 2012.
59. E. A. Paschos, J.-Y. Yu, and M. Sakuda, “Neutrino production of resonances,” *Phys.*  
*Rev.*, vol. D69, p. 014013, 2004.
60. A. Bodek and T. Cai, “Comparison of optical potential for nucleons and  $\Delta$  resonances:  
In electron scattering from nuclear targets,” *Eur. Phys. J.*, vol. C80, no. 7, p. 655, 2020.
61. L. L. Salcedo, E. Oset, M. J. Vicente-Vacas, and C. Garcia-Recio, “Computer Simulation  
of Inclusive Pion Nuclear Reactions,” *Nucl. Phys.*, vol. A484, pp. 557–592, 1988.
62. R. Merenyi, W. A. Mann, T. Kafka, W. Leeson, B. Saitta, J. Schneps, M. Derrick, and  
B. Musgrave, “Determination of pion intranuclear rescattering rates in muon-neutrino  
Ne versus muon-neutrino D interactions for the atmospheric neutrino flux,” *Phys. Rev.*,  
vol. D45, pp. 743–751, 1992.
63. E. Oset and L. L. Salcedo, “ $\Delta$  Selfenergy in Nuclear Matter,” *Nucl. Phys.*, vol. A468,  
pp. 631–652, 1987.
64. O. Lalakulich and U. Mosel, “Pion production in the MiniBooNE experiment,” *Phys.*  
*Rev. C*, vol. 87, no. 1, p. 014602, 2013.
65. E. Hernández, J. Nieves, and M. J. Vicente Vacas, “Single  $\pi$  production in neutrino-  
nucleus scattering,” *Phys. Rev. D*, vol. 87, no. 11, p. 113009, 2013.
66. B. Eberly *et al.*, “Charged Pion Production in  $\nu_\mu$  Interactions on Hydrocarbon at  $\langle E_\nu \rangle =$   
4.0 GeV,” *Phys. Rev.*, vol. D92, no. 9, p. 092008, 2015.
67. C. L. McGivern *et al.*, “Cross sections for  $\nu_\mu$  and  $\bar{\nu}_\mu$  induced pion production on hydro-  
carbon in the few-GeV region using MINERvA,” *Phys. Rev.*, vol. D94, no. 5, p. 052005,  
2016.
68. O. Altinok *et al.*, “Measurement of  $\nu_\mu$  charged-current single  $\pi^0$  production on hydro-  
carbon in the few-GeV region using MINERvA,” *Phys. Rev.*, vol. D96, no. 7, p. 072003,  
2017.
69. D. Coplowe *et al.*, “Probing nuclear effects with neutrino-induced charged-current neu-  
tral pion production,” *Phys. Rev.*, vol. D102, no. 7, p. 072007, 2020.

70. T. Le *et al.*, “Single Neutral Pion Production by Charged-Current  $\bar{\nu}_\mu$  Interactions on Hydrocarbon at  $\langle E_\nu \rangle = 3.6$  GeV,” *Phys. Lett.*, vol. B749, pp. 130–136, 2015.
71. T. Le *et al.*, “Measurement of  $\bar{\nu}_\mu$  Charged-Current Single  $\pi^-$  Production on Hydrocarbon in the Few-GeV Region using MINERvA,” *Phys. Rev.*, vol. D100, no. 5, p. 052008, 2019.
72. P. Stowell *et al.*, “Tuning the GENIE Pion Production Model with MINERvA Data,” *Phys. Rev.*, vol. D100, no. 7, p. 072005, 2019.
73. X.-G. Lu and J. T. Sobczyk, “Identification of nuclear effects in neutrino and antineutrino interactions on nuclei using generalized final-state correlations,” *Phys. Rev.*, vol. C99, no. 5, p. 055504, 2019.
74. M. Rafi Alam, I. Ruiz Simo, M. Sajjad Athar, and M. J. Vicente Vacas, “Weak Kaon Production off the Nucleon,” *Phys. Rev. D*, vol. 82, p. 033001, 2010.
75. C. M. Marshall *et al.*, “Measurement of  $K^+$  production in charged-current  $\nu_\mu$  interactions,” *Phys. Rev.*, vol. D94, no. 1, p. 012002, 2016.
76. C. M. Marshall *et al.*, “Measurement of neutral-current  $K^+$  production by neutrinos using MINERvA,” *Phys. Rev. Lett.*, vol. 119, no. 1, p. 011802, 2017.
77. A. Filkins *et al.*, “Double-differential inclusive charged-current  $\nu_\mu$  cross sections on hydrocarbon in MINERvA at  $\langle E_\nu \rangle \sim 3.5$  GeV,” *Phys. Rev.*, vol. D101, no. 11, p. 112007, 2020.
78. B. G. Tice *et al.*, “Measurement of Ratios of  $\nu_\mu$  Charged-Current Cross Sections on C, Fe, and Pb to CH at Neutrino Energies 2-20 GeV,” *Phys. Rev. Lett.*, vol. 112, no. 23, p. 231801, 2014.
79. J. Mousseau *et al.*, “Measurement of Partonic Nuclear Effects in Deep-Inelastic Neutrino Scattering using MINERvA,” *Phys. Rev.*, vol. D93, no. 7, p. 071101, 2016.
80. A. Bodek and U.-k. Yang, “Axial and Vector Structure Functions for Electron- and Neutrino- Nucleon Scattering Cross Sections at all  $Q^2$  using Effective Leading order Parton Distribution Functions,” 11 2010.
81. I. C. Cloet, W. Bentz, and A. W. Thomas, “EMC and polarized EMC effects in nuclei,” *Phys. Lett. B*, vol. 642, pp. 210–217, 2006.
82. A. Higuera *et al.*, “Measurement of Coherent Production of  $\pi^\pm$  in Neutrino and Antineutrino Beams on Carbon from  $E_\nu$  of 1.5 to 20 GeV,” *Phys. Rev. Lett.*, vol. 113, no. 26, p. 261802, 2014.
83. A. Mislivec *et al.*, “Measurement of total and differential cross sections of neutrino and antineutrino coherent  $\pi^\pm$  production on carbon,” *Phys. Rev.*, vol. D97, no. 3, p. 032014, 2018.
84. C. Berger and L. M. Sehgal, “PCAC and coherent pion production by low energy neutrinos,” *Phys. Rev.*, vol. D79, p. 053003, 2009.
85. D. Rein and L. M. Sehgal, “Coherent  $\pi^0$  Production in Neutrino Reactions,” *Nucl. Phys.*, vol. B223, pp. 29–44, 1983.
86. D. Rein and L. M. Sehgal, “PCAC and the Deficit of Forward Muons in  $\pi^+$  Production by Neutrinos,” *Phys. Lett.*, vol. B657, pp. 207–209, 2007.
87. S. K. Singh, M. Sajjad Athar, and S. Ahmad, “Nuclear effects in neutrino induced coherent pion production at K2K and MiniBooNE,” *Phys. Rev. Lett.*, vol. 96, p. 241801, 2006.
88. L. Alvarez-Ruso, L. S. Geng, S. Hirenzaki, and M. J. Vicente Vacas, “Coherent pion production in neutrino-nucleus collisions,” in *23rd International Nuclear Physics Conference (INPC 2007)*, 9 2007.
89. Z. Wang *et al.*, “First evidence of coherent  $K^+$  meson production in neutrino-nucleus scattering,” *Phys. Rev. Lett.*, vol. 117, no. 6, p. 061802, 2016.
90. D. Rein, “Diffractive Pion Production in Neutrino Reactions,” *Nucl. Phys.*, vol. B278, pp. 61–77, 1986.
91. J. Wolcott *et al.*, “Evidence for Neutral-Current Diffractive  $\pi^0$  Production from Hydrogen in Neutrino Interactions on Hydrocarbon,” *Phys. Rev. Lett.*, vol. 117, no. 11, p. 111801, 2016.
92. R. Fine, B. Messerly, and K. S. McFarland, “Data Preservation at MINERvA,” 2020.
93. B. Messerly *et al.*, “An Error Analysis Toolkit for Binned Counting Experiments,” 2021.